

## Influence of cobalt substitution on the magnetism of NiBr<sub>2</sub>

Binod K. Rai,<sup>1,\*</sup> Andrew D. Christianson,<sup>1</sup> David Mandrus,<sup>1,2,3</sup> and Andrew F. May<sup>1</sup>

<sup>1</sup>Materials Science and Technology Division, Oak Ridge National Laboratory, Oak Ridge, Tennessee 37831, USA

<sup>2</sup>Department of Physics and Astronomy, University of Tennessee, Knoxville, Tennessee 37996, USA

<sup>3</sup>Department of Materials Science and Engineering, University of Tennessee, Knoxville, Tennessee 37996, USA



(Received 4 December 2018; revised manuscript received 5 February 2019; published 25 March 2019)

Co-substituted Ni<sub>1-x</sub>Co<sub>x</sub>Br<sub>2</sub> ( $0 \leq x \leq 1$ ) single crystals were synthesized using vapor transport. The physical properties of the crystals were characterized by x-ray powder diffraction, magnetization, and specific-heat measurements. Room-temperature x-ray powder diffraction data indicate that a change from the CdCl<sub>2</sub> structure type to the CdI<sub>2</sub> structure type occurs within  $0.56 < x < 0.76$ . NiBr<sub>2</sub> has a commensurate antiferromagnetic phase below  $T_N \approx 46$  K and an incommensurate magnetic ground state below  $T_{IC} \approx 20$  K. Both magnetic transitions are affected by cobalt substitution, and the incommensurate phase transition is present up to at least  $x = 0.56$ . The evolution of magnetism has been studied as a function of cobalt content and is summarized in the temperature-composition phase diagram.

DOI: [10.1103/PhysRevMaterials.3.034005](https://doi.org/10.1103/PhysRevMaterials.3.034005)

### I. INTRODUCTION

Binary transition-metal dihalides  $MX_2$  ( $M$  = transition metal and  $X$  = halogen) are of great interest to the low-dimensional magnetism community because of their novel physics and potential applications [1–3].  $MX_2$  compounds contain triangular nets of transition-metal ions, and a helimagnetic ground state is observed in the few dihalides where long-range interactions are important [4–6]. The dihalides that host the helimagnetic structure have received attention in recent years due to the discovery of the coupling between helimagnetic order and ferroelectric polarization [7–10]. NiBr<sub>2</sub> has recently received renewed interest as a multiferroic [8] and for its potential to host a magnetic vortex state upon chemical substitution [11] or multiple- $q$  states under applied magnetic field [12,13], all of which are associated with its helimagnetic ground state.

NiBr<sub>2</sub> is a magnetic insulator that has a commensurate magnetic structure below an antiferromagnetic transition temperature of  $T_N \approx 48$  K [8,14,15]. The magnetic structure changes from a commensurate one to an incommensurate one below  $T_{IC} \approx 20$  K, and this magnetic ground state is a helical spin structure [6,15]. In both magnetic phases, the moments are oriented within the basal plane of the rhombohedral structure (see Fig. 1). The incommensurate structure is believed to result from a delicate balance between the first-neighbor ferromagnetic exchange constant  $J_1$  and the longer-range antiferromagnetic exchange constants  $J_2$  and  $J_3$  [see Fig. 1(c)] [16–18]. The competition between these exchange constants is affected by external control parameters including magnetic field, pressure, or chemical substitution [14,15,19–24], which destabilize the incommensurate spin structure. An applied magnetic field suppresses  $T_{IC}$ , and the incommensurate phase changes to the commensurate one

around 2.7 T at  $T = 2$  K for  $H \perp c$  [19]. The helimagnetic structure of NiBr<sub>2</sub> is also affected by hydrostatic pressure and it disappears with applied pressure above 10.6 kbar, while the antiferromagnetic phase remains unchanged [22,23].

Chemical substitution studies of NiBr<sub>2</sub> have been reported and a complete Ni-site substitution by other transition metals (Ni<sub>1-x</sub>TM<sub>x</sub>Br<sub>2</sub>,  $TM = \text{Mn, Fe, Zn}$ ) was hindered by solubility limits [14,22,25]. Fe-doping suppresses  $T_N$ , and Fe content greater than  $x \geq 0.112$  is reported to eliminate the incommensurate phase and induce an easy-axis, collinear antiferromagnetic structure [14]. The highest reported Mn content is  $x \approx 0.03$ , which slightly suppresses  $T_{IC}$  without changing  $T_N$  [14]. In Ni<sub>1-x</sub>Zn<sub>x</sub>Br<sub>2</sub>, the highest reported Zn content  $x = 0.08$  slightly suppresses  $T_N$  and  $T_{IC}$ . Interestingly, the propagation vector of the incommensurate structure becomes disordered upon Zn substitution [22,25], and it has been recently proposed that Ni<sub>0.92</sub>Zn<sub>0.08</sub>Br<sub>2</sub> could contain an impurity-driven vortex lattice phase [11]. These results highlight the sensitivity of the incommensurate spin structure of NiBr<sub>2</sub> to chemical perturbation.

To further explore the magnetism of NiBr<sub>2</sub>, we have investigated the impact of cobalt substitution in Ni<sub>1-x</sub>Co<sub>x</sub>Br<sub>2</sub>. CdCl<sub>2</sub> and CdI<sub>2</sub> are the prototypes for the two dominant structure types in the  $MX_2$  family, shown in Fig. 1. In both structure types, triangular nets of transition-metal ions are separated by two planes of halide ions that are weakly bonded by van der Waals forces [2]. The main difference between these structure types is the layer stacking, which is reflected in the lattice centering. NiBr<sub>2</sub> crystallizes in the rhombohedral CdCl<sub>2</sub> structure type with space group  $R\bar{3}m$  [6] and has  $ABC$  layer stacking yielding three NiBr<sub>2</sub> layers per unit cell. CoBr<sub>2</sub> crystallizes in the CdI<sub>2</sub> structure type with space group  $P\bar{3}m1$ , and it has one CoBr<sub>2</sub> layer per unit cell [2,26,27]. Thus, the  $c$ -axis lattice parameter of NiBr<sub>2</sub> is approximately three times that of CoBr<sub>2</sub>. CoBr<sub>2</sub> has a commensurate magnetic structure below  $T_N \approx 19$  K and does not host a helimagnetic ground state [26,27].

\*rairk@ornl.gov

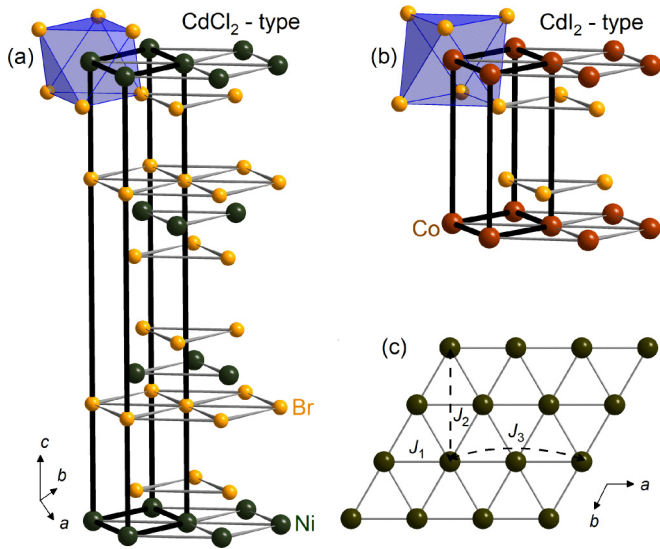


FIG. 1. (a)  $\text{NiBr}_2$  crystal structure with the  $\text{CdCl}_2$  structure type ( $R\bar{3}m$ ). (b)  $\text{CoBr}_2$  crystal structure with the  $\text{CdI}_2$  structure type ( $P\bar{3}m1$ ). In (a) and (b), a single unit cell is outlined and lines connect atoms to aid in viewing. (c) Plan view of a single layer of transition metal with exchange constants  $J_{1,2,3}$  defined.

In this study, single crystals of  $\text{Ni}_{1-x}\text{Co}_x\text{Br}_2$  ( $0 \leq x \leq 1$ ) have been synthesized and characterized using magnetization and specific heat measurements. A composition-induced transition from the  $\text{CdCl}_2$  structure type of  $\text{NiBr}_2$  to the  $\text{CdI}_2$  structure type of  $\text{CoBr}_2$  has been observed within  $0.56 < x < 0.76$  by room-temperature powder x-ray diffraction data. A magnetic phase diagram has been established based on magnetization and specific heat measurements. For samples with the  $\text{CdCl}_2$  structure type,  $T_N$  is continuously suppressed with increasing cobalt concentration. The stability of the incommensurate phase seems to be enhanced for  $x \leq 0.26$ , and signatures of this phase are detected up to  $x = 0.56$ .

## II. EXPERIMENTAL METHODS

Single crystals of  $\text{Ni}_{1-x}\text{Co}_x\text{Br}_2$  ( $0 \leq x \leq 1$ ) were grown from anhydrous  $\text{NiBr}_2$  (99.99% purity) and  $\text{CoBr}_2$  (99.99% purity) using vapor transport.  $\text{NiBr}_2$  and  $\text{CoBr}_2$  were placed in a silica ampoule inside a helium-filled glove box and sealed under vacuum without exposure to air. The ampoules were heated in a horizontal tube furnace at temperatures ranging from  $900^\circ\text{C}$  ( $\text{NiBr}_2$ ) to  $620^\circ\text{C}$  ( $\text{CoBr}_2$ ) for several days, and cooled to room temperature within 1 day. The growths resulted in crystals at the cold end of the ampoule, with crystalline facets that were the cleavage  $ab$  plane. Despite optimizing the growth conditions for each composition, the size of the single crystals decreased with increasing  $x$ ; a representative crystal ( $x \approx 0.31$ ) is shown in inset of Fig. 2(a). The  $\text{Ni}_{1-x}\text{Co}_x\text{Br}_2$  crystals are air sensitive and the sensitivity to air increases as Co content increases. We emphasize that care must be taken to avoid air exposure, especially for large  $x$ , or else anomalous physical properties may be observed below 10 K.

Room-temperature powder x-ray diffraction data were collected in a PANalytical X'Pert Pro MPD diffractometer (Cu

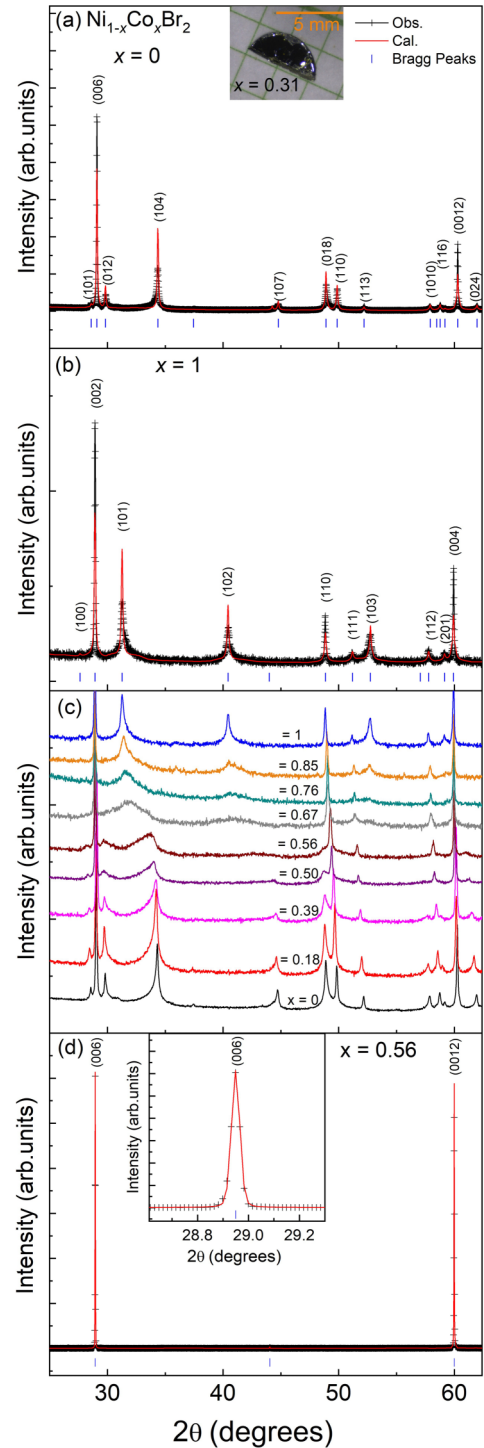


FIG. 2. Room-temperature x-ray powder diffraction pattern (black line + symbol) with Le Bail fit (red line) of (a)  $\text{NiBr}_2$  and (b)  $\text{CoBr}_2$ . Inset of (a): Crystal picture for  $x = 0.31$ . (c) X-ray diffraction data of  $\text{Ni}_{1-x}\text{Co}_x\text{Br}_2$ . (d) A representative diffraction pattern from a facet for  $x = 0.56$ . Inset of (d): Zoom-in view of 006 reflection.

$\text{K}\alpha_1$  radiation). The crystals were mixed with glass powder, and the mixtures were ground into powders using a mortar and pestle inside a helium glove box. The fine powders were sealed in an air-free sample holder. X-ray diffraction data were

TABLE I. The nominal growth composition, the value obtained by EDS, and the corresponding standard deviations (STDEV) that provide the relative error for the EDS measurements.

Nominal	0.10	0.20	0.25	0.30	0.40	0.5	0.55	0.70	0.75	0.80
EDS $x$	0.11	0.18	0.25	0.31	0.39	0.5	0.56	0.67	0.76	0.85
STDEV (%)	1.0	3.8	1.5	2.6	2.0	1.8	1.4	4.0	1.1	2.1

also collected from facets of freshly cleaved single crystals, and these data contain the 00l reflections. The x-ray diffraction data were analyzed with the program FullProf [28] using the Le Bail technique. Energy dispersive x-ray spectroscopy (EDS) was employed to determine the  $x$  values from relative Ni and Co concentrations assuming full transition-metal occupancy; a Hitachi TM3000 with Bruker EDS detector was utilized. EDS was performed on both sides of at least two crystals for each  $x$ , and the EDS values were obtained by averaging the results of at least 20 spots per measurement with error bars being the standard deviation. The  $x$  values provided in this work are the experimental ones obtained from EDS and are reported in Table I. The EDS measurements also provide important guidance on the growth optimization, as samples from growths that were not properly optimized exhibited a large variation in  $x$ . Anisotropic magnetization measurements were performed in a Quantum Design Magnetic Property Measurement System. To identify intrinsic magnetic behavior for the most air-sensitive samples, including  $\text{CoBr}_2$ , the crystals were sealed inside a quartz tube containing helium exchange gas. Specific-heat data were collected in a Quantum Design Physical Property Measurement System.

### III. RESULTS AND DISCUSSION

#### A. Structure

Room-temperature x-ray powder diffraction data are shown in Fig. 2. The  $\text{NiBr}_2$  [see Fig. 2(a)] and  $\text{CoBr}_2$  [see Fig. 2(b)] powder diffraction patterns are well described by the  $\text{CdCl}_2$  structure type and the  $\text{CdI}_2$  structure type, respectively, using Le Bail fitting. Figure 2(c) shows the powder diffraction patterns of  $\text{Ni}_{1-x}\text{Co}_x\text{Br}_2$ . The diffraction data show the change in structure type at room temperature occurs within  $0.56 < x < 0.76$ . This transition is best viewed by tracking the 104 and 102 reflections of  $\text{NiBr}_2$  and  $\text{CoBr}_2$ , respectively.

The asymmetry and broadness of the Bragg reflections increase as  $x$  approaches the change in the structure type. Indeed, the weakest  $h0l$  reflections are fully suppressed near the change in the structure type. The apparent asymmetric and broad Bragg reflections in such layered materials may result from a combination of stacking faults or disorder or strain [29,30]. In our study, the 00l and  $hhl$  peaks obtained from diffraction data are not significantly broadened, even for  $x = 0.67$ . The  $h0l$  reflections are broadened and this suggests stacking disorder contributes most to the broadening [30]. The compositions around the change in the structure type likely have a significant amount of disorder associated with layer stacking, and this makes defining a precise composition where the structure type changes inappropriate because layer stacking is what differentiates the structure types. For the

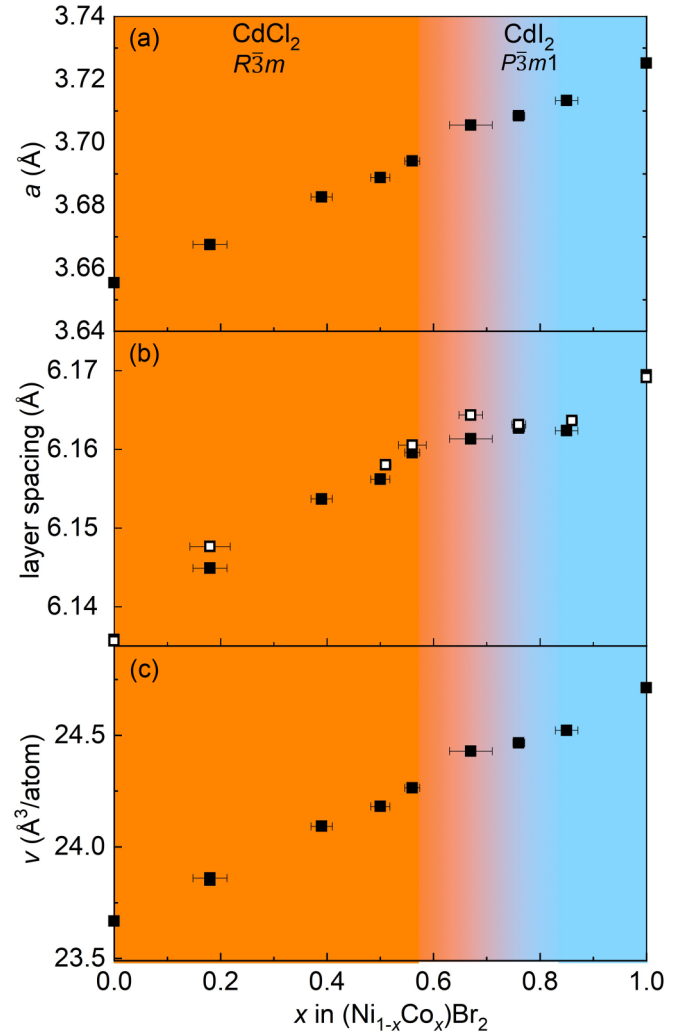


FIG. 3. (a) Lattice parameter  $a$ , (b) layer spacing, and (c) the average volume per atom as a function of  $x$  (obtained from EDS) in  $\text{Ni}_{1-x}\text{Co}_x\text{Br}_2$  at 300 K. The vertical error bars are smaller than the data points. Note: Closed symbols from powder diffraction and open symbols for diffraction data collected from the facets of single crystals. The area where the colors merge represents a region where stacking disorder hinders the ability to define a macroscopic symmetry.

$x = 0.67$  sample where a large degree of stacking disorder and composition variation are evident, we obtained lattice parameters using the  $\text{CdI}_2$  model because it provided the best fitting of the diffraction data. However, near this composition it is probably not reasonable to ascribe a particular structure model.

The change in the lattice parameters as a function of  $x$  is shown in Fig. 3. The  $a$ -axis lattice parameter increases continually from  $x = 0$  to 1 as shown in Fig. 3(a). The layer spacing and the average volume per atom increase with increasing  $x$  similar to the change in the  $a$ -axis lattice parameter [see Figs. 3(b) and 3(c)]. The layer spacing is equal to  $c$  for samples with the  $\text{CdI}_2$  structure type and is equal to  $c/3$  for those with the  $\text{CdCl}_2$  structure type. Le Bail fitting ( $2\theta = 10^\circ\text{--}100^\circ$ ) was performed to obtain the lattice parameters of  $\text{Ni}_{1-x}\text{Co}_x\text{Br}_2$ , and the reported lattice parameters for  $x = 0.56$

and 0.67 were calculated excluding ( $h0l$ ) Bragg reflections from the fitting.

X-ray diffraction data collected from the facets of single crystals are characterized by sharp 00l reflections for all samples examined, including  $x = 0.56$  [shown in Fig. 2(d)]. This suggests the crystals do not have significant macroscopic chemical inhomogeneity or immiscibility. The expansion of the layer spacing obtained by fitting these data is in agreement with that obtained from the powder diffraction data. We note, however, that the  $x = 0.67$  sample has much higher standard deviations in the EDS measurements and the symmetry is not well defined. Thus, it is possible that near  $x = 0.67$  some immiscibility exists that is beyond our resolution.

### B. Magnetic properties

The temperature-dependent anisotropic magnetization  $M$  of  $\text{NiBr}_2$  and  $\text{CoBr}_2$  was measured in an applied magnetic field  $\mu_0 H = 1$  T, and the results are shown in Fig. 4. A broad cusp in the temperature-dependent magnetization  $M/H$  is observed upon cooling, which corresponds to a transition from a paramagnetic phase to a commensurate antiferromagnetic phase. The transition temperatures  $T_N = 46(1)$  K for  $\text{NiBr}_2$  and  $18(1)$  K for  $\text{CoBr}_2$  are determined from peaks in  $d(MT)/dT$  [31]. In addition to  $T_N$  in  $\text{NiBr}_2$ , when  $H \perp c$ , a small decrease in  $M/H$  below  $T \approx 20$  K is observed and corresponds to the onset of the helimagnetic structure. The transition temperature  $T_{IC} = 20(1)$  K is also determined from a peak in  $d(MT)/dT$ .  $T_N$  and  $T_{IC}$  determined from our study are in agreement with previous reports [22,26].  $T_{IC}$  is not observed when  $H \parallel c$  for  $\text{NiBr}_2$ , and it is absent in  $\text{CoBr}_2$ . We note that  $T_{IC}$  of  $\text{NiBr}_2$  is suppressed with applied magnetic field  $H \perp c$  [8].

Neutron diffraction studies on  $\text{NiBr}_2$  and  $\text{CoBr}_2$  reported that the moments align ferromagnetically within a layer and stack antiferromagnetically along the  $c$  axis, and furthermore the studies suggest that the ordered moments orient in the  $ab$  plane [26,32,33]. Despite this similarity from the perspective of neutron diffraction, the measured anisotropy of the induced magnetization is opposite between  $\text{NiBr}_2$  and  $\text{CoBr}_2$  [see Fig. 4(a)]. The temperature-dependent  $M/H$  of both compounds shows Curie-Weiss behavior at high temperature. The effective moments and Weiss temperature  $\theta_W$  are extracted from a linear fit (red line) of the inverse magnetic susceptibility  $H/M$  at  $150 \text{ K} \leq T \leq 350 \text{ K}$ , as shown in Figs. 4(b) and 4(c). For  $\text{NiBr}_2$ , the experimental effective moment is  $3.25 \mu_B/\text{Ni}$ , which is larger than the calculated spin-only ( $S = 1$ ) effective moment of  $2.83 \mu_B/\text{Ni}^{+2}$ . The experimental effective moment suggests some orbital contribution to the moment, which is consistent with the reported  $g \approx 2.2$  of  $\text{NiBr}_2$  [34]. For  $\text{NiBr}_2$ , we obtained  $\theta_W$  of 48 K and 51 K for  $H \perp c$  and  $H \parallel c$ , respectively, indicating ferromagnetic correlations in the paramagnetic state that are consistent with a previous report [24]. For  $\text{CoBr}_2$ , the experimental effective moment of  $5.53 \mu_B/\text{Co}$  is larger than the calculated spin-only value ( $3.87 \mu_B/\text{Co}^{+2}$ ), and a similar effective moment of  $5.29 \mu_B/\text{Co}$  has been reported in isostructural  $\text{CoCl}_2$  [35]. The  $\theta_W$  are 7 K and  $-81$  K for  $H \perp c$  and  $H \parallel c$ , respectively, and this behavior may be driven by single-ion anisotropy and/or anisotropic exchange interactions [36].

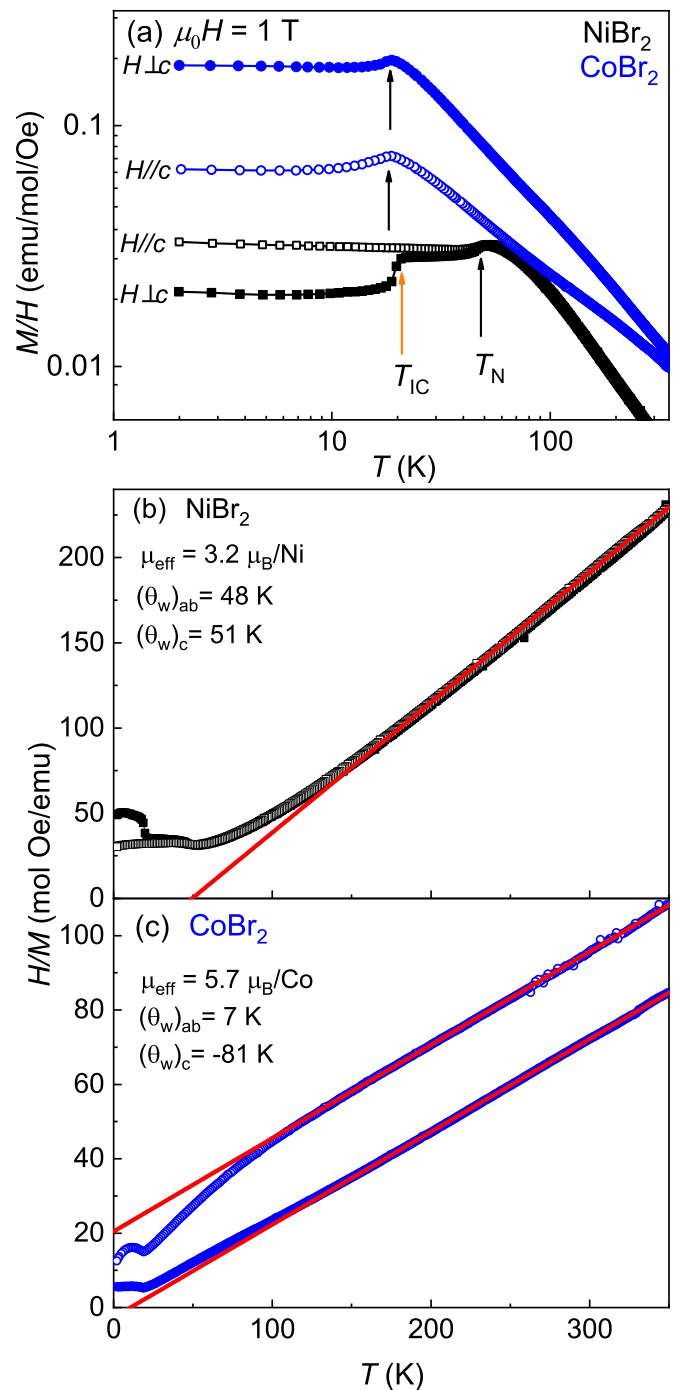


FIG. 4. (a) Temperature-dependent magnetization  $M/H$  collected upon cooling in an applied magnetic field  $\mu_0 H = 1$  T for  $\text{NiBr}_2$  (black) and  $\text{CoBr}_2$  (blue). Temperature-dependent inverse magnetic susceptibility  $H/M$  for (b)  $\text{NiBr}_2$  and (c)  $\text{CoBr}_2$ , with the Curie-Weiss fit between  $150 \text{ K} \leq T \leq 350 \text{ K}$  shown by red line.

We have so far examined the temperature-dependent magnetization for  $\text{NiBr}_2$  and  $\text{CoBr}_2$ . We now examine the impact of cobalt content on the magnetic properties. As shown in Figs. 5(a) and 5(b), the commensurate phase transition at  $T_N$  of  $\text{Ni}_{1-x}\text{Co}_x\text{Br}_2$  is continually suppressed up to  $x = 0.56$ , while a partial Ni substitution leads to an enhancement of  $T_N$  for  $\text{CoBr}_2$ . For  $H \perp c$ , the incommensurate phase transition



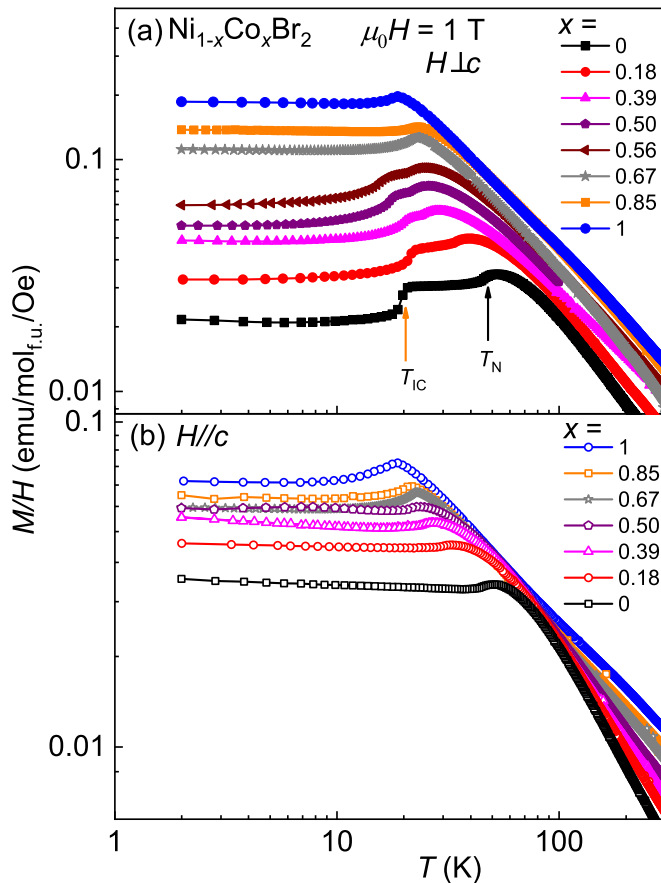


FIG. 5. Temperature-dependent magnetization of  $\text{Ni}_{1-x}\text{Co}_x\text{Br}_2$  collected upon cooling in an applied magnetic field  $\mu_0 H = 1$  T for (a)  $H \perp c$  and (b)  $H \parallel c$ .

[ $T_{\text{IC}} = 20(1)$  K] of  $\text{NiBr}_2$  is first slightly enhanced with Co substitution and is last detected for  $x = 0.56$  [see in Fig. 5(a)].

The isothermal magnetization  $M(H)$  at  $T = 2$  K is shown in Fig. 6. For a given magnetic field,  $M$  of  $\text{NiBr}_2$  [left axis in Fig. 6(a)] is smaller than  $M$  of  $\text{CoBr}_2$  [right axis in Fig. 6(a)]. The induced magnetic moments are not saturated for  $\mu_0 H = 6$  T, and the maximum moment  $M(\mu_0 H = 6 \text{ T}, 2 \text{ K})$  increases continually from  $x = 0$  to 1. For  $\text{NiBr}_2$ , a magnetic anomaly around  $\mu_0 H_c = 2.7$  T is observed for  $H \perp c$  (closed symbols), but it is absent for  $H \parallel c$  (open symbols). The anomaly is related to a transition from the helimagnetic structure to the commensurate antiferromagnetic structure [8,15]. The observed magnetic hysteresis on increasing and decreasing magnetic fields [see in Fig. 6(b)] is consistent with previous reports [8,23], and suggests a first-order transition. Recently, Tokunaga *et al.* investigated multiferroic properties in  $\text{NiBr}_2$  and reported a spontaneous polarization below  $T_{\text{IC}}$  [8]. The ferroelectric transition disappeared above  $H_c$ , and the hysteresis may be related to magnetostructural domain movement.

Specific heat  $C_p(T)$  of  $\text{Ni}_{1-x}\text{Co}_x\text{Br}_2$  at  $\mu_0 H = 1$  T is shown in Fig. 7. Strong anomalies are observed at  $T = 44.6(2)$  K and  $T = 18.4(2)$  K for  $\text{NiBr}_2$  and  $\text{CoBr}_2$ , respectively, which are consistent with  $T_{\text{N}}$  observed from temperature-dependent  $M/H$ . The commensurate-incommensurate phase transition observed in the magnetization for  $\text{NiBr}_2$  is also observed in  $C_p(T)$  as a weak anomaly

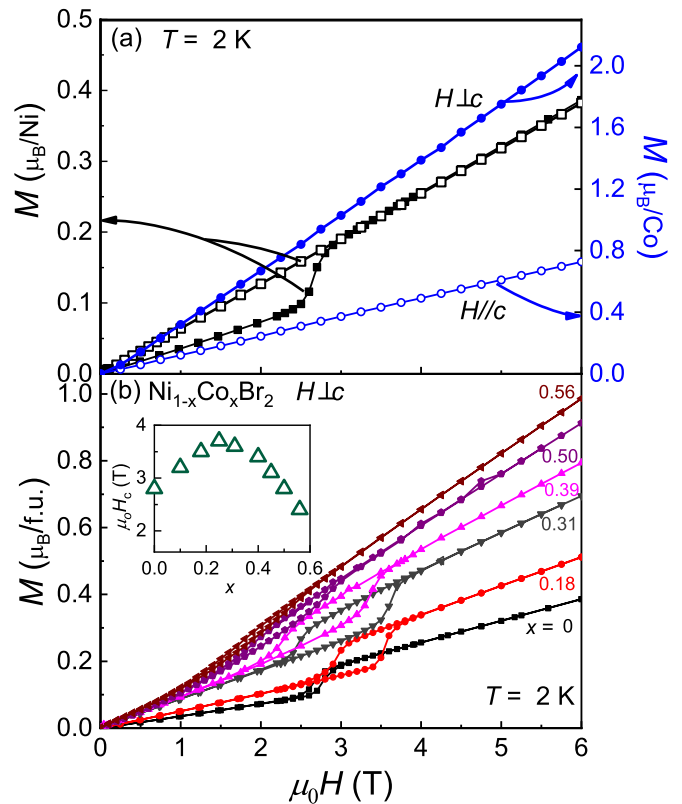


FIG. 6. Isothermal magnetization  $M(H)$  at  $T = 2$  K. (a)  $M(H)$  of  $\text{NiBr}_2$  (left axis) and  $\text{CoBr}_2$  (right axis) for  $H \perp c$  (closed symbols) and  $H \parallel c$  (open symbols). (b)  $M(H)$  for selected compositions of  $\text{Ni}_{1-x}\text{Co}_x\text{Br}_2$  with  $H \perp c$ . Inset: The critical magnetic field as a function of  $x$  determined from a peak in  $dM/dH$  for increasing applied magnetic field.

around  $T \approx 20$  K (see in the inset of Fig. 7). We note that similar behavior was observed at  $T_{\text{N}}$  for specific heat in  $H = 0$ , though the transition at  $T_{\text{IC}}$  was only observed in  $C_p(T)$  with an applied magnetic field  $H \perp c$  and thus results for

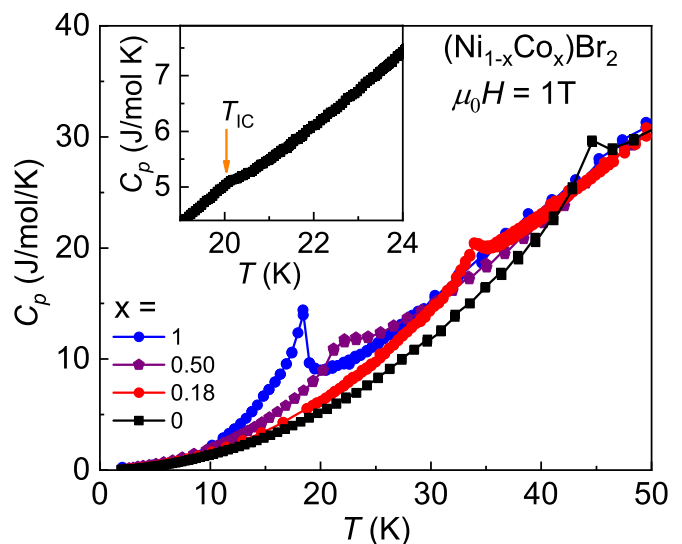


FIG. 7. Specific heat  $C_p(T)$  for  $\text{Ni}_{1-x}\text{Co}_x\text{Br}_2$  for  $\mu_0 H = 1$  T applied within the  $ab$  plane. Inset: A small anomaly observed at  $T_{\text{IC}}$ .

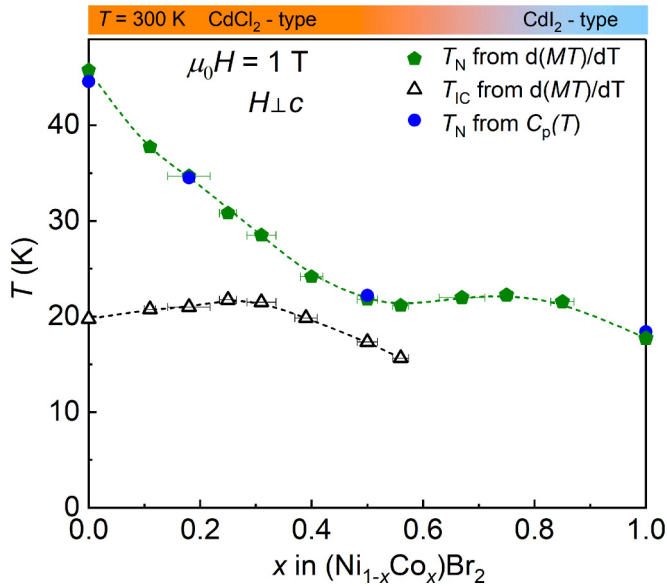


FIG. 8. Temperature-composition phase diagram of magnetic transitions in  $\text{Ni}_{1-x}\text{Co}_x\text{Br}_2$  for  $H \perp c$  at  $\mu_0 H = 1$  T. The dashed lines guide the eye. The colored bar at the top of the graph represents the structural-phase diagram established from room-temperature x-ray diffraction data.

$\mu_0 H = 1$  T are shown.  $C_p(T)$  measurements were used to verify  $T_N$  of a few  $\text{Ni}_{1-x}\text{Co}_x\text{Br}_2$  compositions.

The magnetic transitions of the  $\text{Ni}_{1-x}\text{Co}_x\text{Br}_2$  series derived from peaks in  $C_p(T)$  and  $d(MT)/dT$  [31] are summarized in the temperature-composition phase diagram shown in Fig. 8. Both magnetic transitions of  $\text{NiBr}_2$  are affected by Co substitution. The commensurate phase transition is continually suppressed from  $T_N \approx 46$  K for  $x = 0$  to  $T_N \approx 21$  K for  $x = 0.56$ . A slight enhancement of  $T_N$  for  $\text{CoBr}_2$  is observed with a partial Ni substitution, and a local maximum of  $T_N$  occurs near  $x = 0.76$ . Interestingly,  $T_{IC}$  shows a slight enhancement for small  $x$ , reaching a maximum at  $T_{IC} = 22(1)$  K for  $x = 0.26$  and then finally  $T_{IC}$  is suppressed beyond detection for  $x > 0.56$  at  $\mu_0 H = 1$  T. The evolution of  $H_c$  as a function of cobalt content in  $M(H)$  measurements follows a similar trend as  $T_{IC}$  in temperature-dependent  $M/H$ , indicating a strong correlation between  $H_c$  and  $T_{IC}$ .

The presence of  $T_{IC}$  up to at least  $x = 0.56$  is robust compared to the behavior observed for other transition-metal substitutions in  $\text{NiBr}_2$ . In contrast, the incommensurate magnetic structure of  $\text{NiBr}_2$  disappears by  $x = 0.112$  in  $\text{Ni}_{1-x}\text{Fe}_x\text{Br}_2$  [14], although the  $\text{CdCl}_2$  structure type is retained up to  $x = 0.41$ . Interestingly,  $\text{Ni}_{1-x}\text{Fe}_x\text{Br}_2$  with the helimagnetic structure and a finite easy-axis anisotropy is predicted to host magnetic-field-induced skyrmions [37]. Moreover, a neutron scattering study on  $\text{Ni}_{0.92}\text{Zn}_{0.08}\text{Br}_2$  observed a ring of magnetic scattering in

the  $a^*b^*$  plane around  $(00\frac{3}{2})$  and  $(10\frac{1}{2})$  resulting from a disordered propagation vector of the helimagnetic structure [15]. It has been proposed that the ground state associated with this magnetic scattering is an impurity-driven vortex lattice phase [11,38]. These experimental and theoretical results highlight the relevance of using chemical substitution in  $\text{NiBr}_2$  to tune the exotic ground states [11,37]. As such,  $\text{Ni}_{1-x}\text{Co}_x\text{Br}_2$  with the  $\text{CdCl}_2$  structure type is a strong candidate to inspect for nontrivial spin textures such as the magnetic vortex lattice phase or other multiple- $q$  spin textures. Examining the nature of the magnetic ground state of  $\text{Ni}_{1-x}\text{Co}_x\text{Br}_2$  and the correlation between  $T_{IC}$  and  $H_c$  requires additional characterization such as neutron scattering, which is underway.

#### IV. CONCLUSIONS

We synthesized single crystals of  $\text{Ni}_{1-x}\text{Co}_x\text{Br}_2$  ( $0 \leq x \leq 1$ ) using vapor transport. A composition-induced transition from the  $\text{CdCl}_2$  structure type of  $\text{NiBr}_2$  to the  $\text{CdI}_2$  structure type of  $\text{CoBr}_2$  occurs within  $0.56 < x < 0.76$  at 300 K. The in-plane lattice parameter, layer spacing, and the average volume per atom continually increase with  $x$ . For  $\text{Ni}_{1-x}\text{Co}_x\text{Br}_2$  with the  $\text{CdCl}_2$  structure type, increasing the cobalt content leads to a suppression of the commensurate antiferromagnetic phase transition of  $\text{NiBr}_2$ . The transition temperature to the incommensurate phase is first slightly enhanced with cobalt substitution, then it is suppressed and last detected for  $x = 0.56$ . The presence of  $T_{IC}$  up to at least  $x = 0.56$  indicates that the delicate balance between ferromagnetic and antiferromagnetic exchange constants is perhaps still satisfied. Given that  $\text{Ni}_{1-x}\text{Co}_x\text{Br}_2$  with the  $\text{CdCl}_2$  structure type has both  $T_N$  and  $T_{IC}$  transitions in common with  $\text{NiBr}_2$ , which hosts the helimagnetic spin structure, these compositions appear as promising candidates in the ongoing search for topologically nontrivial spin textures.

#### ACKNOWLEDGMENTS

This research was supported by the U.S. Department of Energy, Office of Science, Basic Energy Sciences, Materials Sciences and Engineering Division. We thank D. Parker and C. D. Batista for helpful discussions.

This manuscript has been authored by UT-Battelle, LLC under Contract No. DE-AC05-00OR22725 with the U.S. Department of Energy. The United States Government retains and the publisher, by accepting the article for publication, acknowledges that the United States Government retains a non-exclusive, paid-up, irrevocable, world-wide license to publish or reproduce the published form of this manuscript, or allow others to do so, for United States Government purposes. The Department of Energy will provide public access to these results of federally sponsored research in accordance with the DOE Public Access Plan [39].

[1] M. Mushtaq, Y. Zhou, and X. Xiang, *RSC Adv.* **7**, 22541 (2017).  
 [2] M. A. McGuire, *Crystals* **7**, 121 (2017).

[3] P. Chen, J.-Y. Zou, and B.-G. Liu, *Phys. Chem. Chem. Phys.* **19**, 13432 (2017).

- [4] S. R. Kuindersma, J. P. Sanchez, and C. Haas, *Physica B* **111**, 231 (1981).
- [5] K. Iio, H. Masuda, H. Tanaka, and K. Nagata, *J. Magn. Magn. Mater.* **90-91**, 265 (1990).
- [6] A. Adam, D. Billerey, C. Terrier, R. Mainard, L. P. Regnault, J. Rossat-Mignod, and P. Mériel, *Solid State Commun.* **35**, 1 (1980).
- [7] T. Kurumaji, S. Seki, S. Ishiwata, H. Murakawa, Y. Tokunaga, Y. Kaneko, and Y. Tokura, *Phys. Rev. Lett.* **106**, 167206 (2011).
- [8] Y. Tokunaga, D. Okuyama, T. Kurumaji, T. Arima, H. Nakao, Y. Murakami, Y. Taguchi, and Y. Tokura, *Phys. Rev. B* **84**, 060406(R) (2011).
- [9] X. Wu, Y. Cai, Q. Xie, H. Weng, H. Fan, and J. Hu, *Phys. Rev. B* **86**, 134413 (2012).
- [10] T. Kurumaji, S. Seki, S. Ishiwata, H. Murakawa, Y. Kaneko, and Y. Tokura, *Phys. Rev. B* **87**, 014429 (2013).
- [11] S.-Z. Lin, S. Hayami, and C. D. Batista, *Phys. Rev. Lett.* **116**, 187202 (2016).
- [12] T. Okubo, S. Chung, and H. Kawamura, *Phys. Rev. Lett.* **108**, 017206 (2012).
- [13] S. Babu, K. Prokeš, Y. K. Huang, F. Radu, and S. K. Mishra, *J. Appl. Phys.* **125**, 093902 (2019).
- [14] M. W. Moore and P. Day, *J. Solid State Chem.* **59**, 23 (1985).
- [15] P. Day, M. W. Moore, C. Wilkinson, and K. R. A. Ziebeck, *J. Phys. C: Solid State Phys.* **14**, 3423 (1981).
- [16] E. Rastelli, A. Tassi, and L. Reatto, *Physica B+C* **97**, 1 (1979).
- [17] I. H. Odisho and H. M. Al-Dorry, *J. Phys.: Condens. Matter.* **1**, 6551 (1989).
- [18] A. O. Leonov and M. Mostovoy, *Nat. Commun.* **6**, 8275 (2015).
- [19] K. Katsumata, K. Sugiyama, and M. Date, *J. Phys. Soc. Jpn.* **52**, 3312 (1983).
- [20] H. Yoshiyama, N. Suzuki, and K. Motizuki, *J. Phys. C* **17**, 713 (1984).
- [21] H. Yoshiyama, N. Suzuki, and K. Motizuki, *J. Magn. Magn. Mater.* **54-57**, 1347 (1986).
- [22] P. Day and C. Vettier, *J. Phys. C* **14**, L195 (1981).
- [23] A. Adam, D. Billerey, C. Terrier, H. Bartholin, L. P. Regnault, and J. Rossat-Mignod, *Phys. Lett. A* **84**, 24 (1981).
- [24] L. P. Régnault, J. Rossat-Mignod, A. Adam, D. Billerey, and C. Terrier, *J. Phys.* **43**, 1283 (1982).
- [25] M. W. Moore, T. E. Wood, and P. Day, *J. Chem. Soc., Faraday Trans. 2* **77**, 1611 (1981).
- [26] M. K. Wilkinson, J. W. Cable, E. O. Wollan, and W. C. Koehler, *Phys. Rev.* **113**, 497 (1959).
- [27] K. Katsumata, J. Tuchendler, and S. Legrand, *Phys. Rev. B* **30**, 1377 (1984).
- [28] J. Rodriguez-Carvajal, *Physica B* **192**, 55 (1993).
- [29] S. Hendricks and E. Teller, *J. Chem. Phys.* **10**, 147 (1942).
- [30] T. N. Ramesh, R. S. Jayashree, and P. V. Kamath, *Clays Clay Miner.* **51**, 570 (2003).
- [31] M. E. Fisher, *Philos. Mag.* **7**, 1731 (1962).
- [32] P. Day, A. Dinsdale, E. R. Krausz, and D. J. Robbins, *J. Phys. C* **9**, 2481 (1976).
- [33] P. Day, *Acc. Chem. Res.* **21**, 250 (1988).
- [34] J. Tuchendler and K. Katsumata, *Solid State Commun.* **55**, 769 (1985).
- [35] C. Starr, F. Bitter, and A. R. Kaufmann, *Phys. Rev.* **58**, 977 (1940).
- [36] D. C. Johnston, *Phys. Rev. B* **95**, 094421 (2017).
- [37] S. Hayami, S.-Z. Lin, and C. D. Batista, *Phys. Rev. B* **93**, 184413 (2016).
- [38] C. D. Batista, S. Lin, S. Hayami, and Y. Kamiya, *Rep. Prog. Phys.* **79**, 084504 (2016).
- [39] <http://energy.gov/downloads/doe-public-access-plan>.